p-GaN/n-ZnO Heterojunction Nanowires: Optoelectronic Properties and the Role of Interface Polarity

Fabian Schuster,[†,*] Bernhard Laumer,[†] Reza R. Zamani,[‡,§] Cesar Magén,[⊥,∥] Joan Ramon Morante,[§,#] Jordi Arbiol,[‡,▽] and Martin Stutzmann[†,*]

[†]Walter Schottky Institut, Technische Universität München, Am Coulombwall 4, 85748 Garching, Germany, [‡]Institut de Ciència de Materials de Barcelona, ICMAB-CSIC, Campus de la UAB, 08193 Bellaterra, Catalonia Spain, [§]Catalonia Institute for Energy Research, IREC, 08930 Sant Adrià del Besòs, Catalonia Spain, [⊥]Laboratorio de Microscopías Avanzadas (LMA), Instituto de Nanociencia de Aragon (INA) and Departamento de Física de la Materia Condensada, Universidad de Zaragoza, 50018 Zaragoza, Aragon, Spain, [∥]Fundación ARAID, 50018 Zaragoza, Aragon, Spain, [#]Departament d'Electronica, Universitat de Barcelona, 08028 Barcelona, Catalonia Spain, and [▽]Institució Catalana de Recerca i Estudis Avançats (ICREA), 08010 Barcelona, Catalonia Spain

ABSTRACT In this work, simulations of the electronic band structure of a p-GaN/n-ZnO heterointerface are presented. In contrast to homojunctions, an additional energy barrier due to the type-II band alignment hinders the flow of majority charge carriers in this heterojunction. Spontaneous polarization and piezoelectricity are shown to additionally affect the band structure and the location of the recombination region. Proposed as potential UV-LEDs and laser diodes, p-GaN/n-ZnO heterojunction nanowires were fabricated by plasma-assisted molecular beam epitaxy (PAMBE). Atomic resolution annular bright field scanning transmission electron microscopy (STEM) studies reveal an abrupt and defect-free heterointerface with a polarity inversion from N-polar GaN to Zn-polar ZnO. Photoluminescence measurements show strong excitonic UV emission originating from the ZnO-side of the interface as well as stimulated emission in the case of optical pumping above a threshold of 55 kW/cm^2.

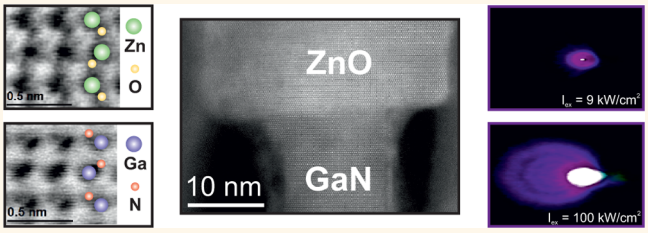

KEYWORDS: nanowires · GaN · ZnO · heterojunction · interface · polarity · molecular beam epitaxy · ABF STEM

The idea of combining ZnO and GaN was originally motivated by the desire to find suitable substrates for heteroepitaxy. As both materials share the wurtzite crystal structure with similar lattice parameters (Table 1), heteroepitaxy of ZnO on GaN[1,2] and *vice versa*[3] was reported to yield better results compared to the usual substrates like sapphire due to low structural defect densities. At that time, both material systems (group-III-nitrides and group-II-oxides) were considered to be well suited for optoelectronic devices and, thus, extensively studied. The higher exciton binding energy in ZnO seemed to be a big advantage with respect to high-power, light-emitting devices operating above room temperature. However, the problems with stable and reproducible p-type doping in ZnO was decisive that, in the end, GaN turned out to be more appropriate for device fabrication.

The realization that bipolar ZnO devices founder on the lack of p-type doping is widely accepted by now. As a consequence, applications for ZnO will either stay confined to unipolar devices such as field effect transistors and sensors or, in combination with a suitable p-type material, may be used in bipolar heterojunctions. It is obvious to consider GaN as the perfect p-type supplement. Thus, p-GaN/n-ZnO heterojunctions have been studied by many groups with respect to electroluminescence, which was reported to originate either from the GaN-side[4] or the ZnO-side[5−7] of the interface. To settle this matter, intrinsic ZnO nanorods were introduced to the interface region to form p-GaN/i-ZnO/n-ZnO structures. This indeed proved advantageous in terms of efficiency; however, emission wavelengths still suggested recombination on the p-GaN-side[8,9] with wavelengths around 430 nm due to deep Mg complexes[10] or on the ZnO-side[11,12] of the heterojunction emitting at around 380 nm. Additionally, Yang *et al.* reported a strong impact of external strain

* Address correspondence to Fabian.Schuster@wsi.tum.de, Stutz@wsi.tum.de.

Received for review November 28, 2013 and accepted April 10, 2014.

Published online April 10, 2014
10.1021/nn406134e

TABLE 1. Material Parameters of Wurtzite GaN and ZnO with ∥ and ⊥ Indicating Directions Parallel and Perpendicular to the *c*-Axis[a,20−28]

parameter	GaN	ref	ZnO	ref
E_{gap}(0K)[eV]	3.510	20	3.434	21
$E_{exciton}$[eV]	0.025	22	0.059	23
c [Å]	5.185	20	5.213	21
a [Å]	3.189	20	3.246	21
$m^*_{e,\perp}$	0.20	20	0.24	24
$m^*_{e,\parallel}$	0.20	20	0.28	24
$m^*_{hh,\perp}$	1.60	25	0.54	24
$m^*_{hh,\parallel}$	1.10	25	2.74	24
$m^*_{lh,\perp}$	0.15	25	0.55	24
$m^*_{lh,\parallel}$	1.10	25	3.03	24
$m^*_{so,\perp}$	1.10	25	1.12	24
$m^*_{so,\parallel}$	0.15	25	0.27	24
$\varepsilon_\perp$	9.5	22	7.77	26
$\varepsilon_\parallel$	10.4	22	8.91	26
P_{Sp} [C/m^2]	−0.034	20	−0.057	27
e_{33} [C/m^2]	0.73	22	1.34	28
e_{31} [C/m^2]	−0.36	22	−0.57	28

[a] Effective masses are given in terms of m_0.

on the electroluminescence spectrum[7] while Zhang *et al.* observed an unexpected charge trapping effect when illuminating a forward biased heterojunction LED with UV light.[9]

Despite of apparently contradicting experimental results, no systematic analysis of the band structure in such heterostructures has been published up to now. Therefore, the first part of this article is dedicated to simulations of the electronic band structure of p-GaN/n-ZnO heterostructures with a special focus on polarity issues to develop a deeper understanding of the processes taking place at the interface. In the second part, the experimental findings obtained from structural and optical characterization of p-GaN/n-ZnO heterojunction nanowires are presented and compared to the simulations.

SIMULATION AND POLARITY

Before discussing GaN/ZnO heterostructures, the effect of spontaneous polarization in wurtzite materials is briefly summarized. Figure 1 shows the O^{2-} anion which is surrounded by four tetrahedrally coordinated Zn^{2+} cations. As the lattice parameters in real ZnO crystals deviate from the theoretical ratio $c/a = (8/3)^{1/2}$, dipole moments are induced which do not cancel each other along the *c*-direction and, consequently, give rise to the so-called spontaneous polarization. The same applies for other wurtzite materials such as GaN, AlN, and InN and induces sheet charges at all polar or semipolar surfaces and interfaces. Obviously, these materials are in general also piezoelectric, which means that the electronic properties sensitively react to strain. All these contributions have to be considered for modeling the heterointerface between GaN and ZnO, where the orientation of the

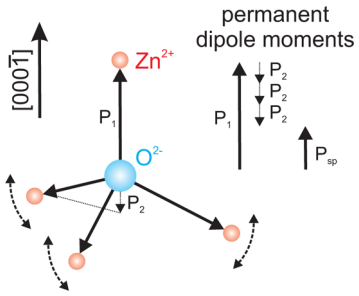

Figure 1. Tetrahedron in a wurtzite ZnO crystal with permanent dipole moments that do not compensate each other. The effect is induced by the strongly ionic character of the bonds and deviations of the *c*/*a* ratio from the ideal value.

two wurtzite lattices with respect to each other will play an important role.

The electronic band structure of the p-GaN/n-ZnO heterointerface was simulated with the help of the **nextnano**[3] software package.[13] Figure 2a shows the basic type-II band lineup of the two materials based on the theoretical valence band offset (VBO) of 1.3 eV.[14] As the published experimental results are 0.8 eV[15] and 0.9 eV,[16] this parameter contains some uncertainty. Nevertheless, the theoretical value was used for the simulation, since the experimental reports do not account for interface effects. To form a pn-heterodiode, the following doping levels were assumed: Mg acceptors in GaN with a density of 1×10^{17} cm^{-3} and an activation energy of 150 meV[17] and intrinsic donors in ZnO with a density of 1×10^{17} cm^{-3} and an activation energy of 35 meV,[18] *e.g.*, hydrogen. The applied material parameters for GaN and ZnO are summarized in Table 1. To account for the internal strain present in the vicinity of such a heterointerface, which induces piezoelectric charges, the growth of ZnO on GaN is considered here. Therefore, ZnO is assumed to grow pseudomorphically for the first monolayers and then relax its biaxial strain linearly over the following 100 nm. The strain tensor components for the growth in a polar direction can be seen in Figure 2a, where $e_{xx} = e_{yy} = (a_{GaN} - a_{ZnO})/a_{ZnO} = -0.0176$ and $e_{zz} = (-2C_{13}/C_{33})e_{xx} = 0.0094$ are connected *via* elastic constants taken from Polian *et al.*[19] It should be noted that this strain tensor is not correct for growth along a nonpolar direction and depends on the actual growth direction, *e.g.*, [10$\bar{1}$0] or [11$\bar{2}$0]. To keep it simple, strain was not considered for nonpolar directions, which is a reasonable assumption as no piezoelectric effect is present in a nonpolar direction anyway.

The simulation sequence was started by the input of the strain tensor to evaluate piezoelectric charges and spontaneous polarization charges at the interface. Then, the Schödinger and Poisson equations were solved self-consistently with applied Neumann boundary conditions $\partial\phi/\partial z = 0$, where z is the growth direction, to enforce a vanishing electric field on both sides

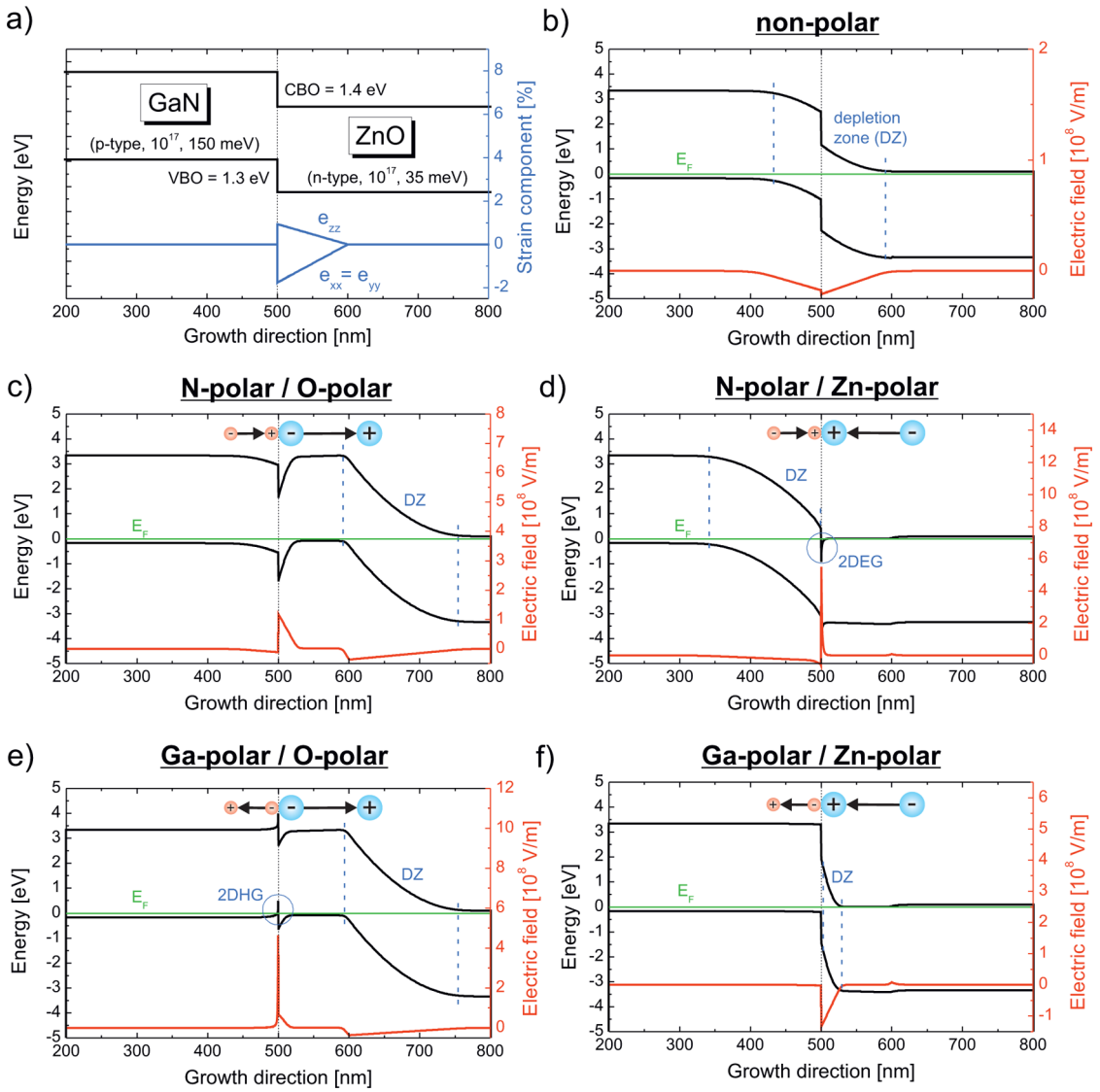

Figure 2. (a) Basic band lineup of a GaN/ZnO heterostructure with the valence band offset (VBO) taken from ref 14. It is assumed that ZnO starts growing pseudomorphically on GaN with linear relaxation of the biaxial strain within 100 nm. The indicated doping levels were used to calculate the band structure of a p-GaN/n-ZnO heterodiode. (b–f) Simulated 1D band structure and electric field for different polarity configurations of the heterostructure, where interface charges due to spontaneous polarization (SPIC) are additionally illustrated. The Fermi levels and depletion zones (DZ) are indicated by green and blue dashed lines, respectively.

toward the bulk. The thermally activated free charge carriers are modeled according to an effective mass approach with Neumann boundary conditions. In all simulations, the Fermi energy (E_F) is set to zero and indicated by the green line.

The calculated 1D band structure, namely, the lowest conduction band energy level and the highest valence band (heavy hole) at the Γ point of the Brillouin zone, is presented together with the electric field across the heterointerface in Figure 2b–f for different polarity configurations. The light hole and split-off valence bands are not shown for better overview. First, the results obtained for a nonpolar p-GaN/n-ZnO heterostructure are depicted in Figure 2b. The interface in this heterostructure is dominated by the type-II alignment of the two materials, where CBO and VBO form energetic barriers for electrons and holes to cross the interface. As these barriers have nearly the same height, the depletion zone (DZ) is formed almost symmetrically on both sides of the heterointerface. In contrast to a homodiode, the additional barrier has to be overcome by the majority charge carriers in forward direction, leading to a shift of the turn-on voltage to higher values. In reverse bias, however, the barriers are advantageous to minimize leakage current and prevent a breakthrough of the heterodiode. Thus, a nonpolar p-GaN/n-ZnO heterojunction LED, which to our knowledge has not yet been reported, probably needs higher driving voltages as its homojunction counterpart for the charge carriers to cross the interface, obviously at the expense of device efficiency.

The situation becomes more complicated for polar heterostructures (Figure 2c−f), where GaN can be either N-polar or Ga-polar and ZnO either O-polar or Zn-polar, leading to interface charges due to both piezoelectricity and spontaneous polarization. The first effect induces two complementary charge densities in the compressively strained ZnO: one located directly at the ZnO-side of the heterointerface where the ZnO starts to grow pseudomorphically (**p**iezoelectric **i**nterface **c**harge, PIC) and the other continuously distributed over the adjacent 100 nm strain relaxation region (**p**iezoelectric **d**istributed **c**harge, PDC). In the region where ZnO reaches its equilibrium lattice parameters, no more piezoelectric charges are present. For O-polar (Zn-polar) ZnO, the PIC is positive (negative) and the corresponding negative (positive) PDC is homogeneously distributed over the relaxation region. The second effect of spontaneous polarization is caused not by strain but by the change in material and induces an additional interface charge depending on the four possible polarity combinations of GaN and ZnO (**s**pontaneous **p**olarization **i**nterface **c**harge, SPIC). This is illustrated by the alignment of the permanent dipole moments in GaN and ZnO in Figure 2c−f. In the following, the four configurations of polar p-GaN/n-ZnO heterostructures are discussed.

In the first polar configuration, the permanent dipole moments in N-polar GaN and O-polar ZnO point in the same direction (Figure 2c), so the discontinuity in spontaneous polarization at the interface is rather small and results in a moderate negative SPIC (−0.023 C/m^2) which is counteracted by a stronger positive PIC (+0.032 C/m^2). This leads to a downward band bending in the vicinity of the interface. Nevertheless, holes can tunnel through the interface region as they are attracted by the negative PDC region (−0.032 C/m^2). As a consequence, the depletion region of the pn-junction is shifted away from the interface deep into the ZnO as depicted in Figure 2c. Therefore, recombination in n-ZnO is expected under forward bias which would result in an electroluminescence wavelength of around 380 nm.

The second configuration to consider is a heterostructure of N-polar GaN and Zn-polar ZnO, where the polarity is inverted from anion to cation polarity (Figure 2d). Here, the dipole moments point in opposite directions, leading to a maximum discontinuity at the interface and a very large positive SPIC (+0.091 C/m^2) which cannot be compensated by a moderate negative PIC (−0.032 C/m^2) in Zn-polar ZnO. This leads to a massive electron accumulation at the interface which drags the conduction band potential well below the Fermi level and, consequently, results in the formation of a two-dimensional electron gas (2DEG) on the ZnO-side of the interface. As holes cannot overcome the high potential barrier at the interface and are additionally repelled by the positive PDC region (+0.032 C/m^2), the depletion region is shifted into the p-GaN region. Thus, in light-emitting devices a recombination on the p-GaN side can be expected under forward bias. Furthermore, this configuration might be interesting for planar field effect transistors, as the electron confinement is much stronger compared to widely used AlGaN/GaN heterostructures.

The third configuration composed of Ga-polar GaN and O-polar ZnO (Figure 2e), which represents also an inverted polarity, forms a strongly negative SPIC (−0.091 C/m^2) which is counteracted only by a moderate positive PIC (+0.032 C/m^2) and, thus, induces the formation of a two-dimensional hole gas (2DHG) on the GaN-side of the interface. Analogue to Figure 2c, the negative PDC region (−0.032 C/m^2) attracts holes to tunnel through the interface into the ZnO side, whereas electrons are repelled from the interface, leading to a shift of the depletion region into the ZnO.

The last configuration is Ga-polar GaN and Zn-polar ZnO (Figure 2f) forming a moderate positive SPIC (+0.023 C/m^2) counteracted by a larger negative PIC (−0.032 C/m^2). The resulting negative potential repels electrons from the interface toward the positive PDC region (+0.032 C/m^2). Thus, despite low doping levels, the depletion region is very thin and located directly on the ZnO-side of the interface. This might be exploited for the fabrication of tunnel diodes where thin depletion regions are necessary and usually achieved by degenerate doping levels.

In summary, the analysis of the p-GaN/n-ZnO heterointerface reveals various possibilities of the band structure, mainly depending on the polarity and strain of the two wurtzite materials. For potential applications it is therefore crucial to choose an optimal polarity configuration according to the particular requirements. The realization is then a matter of growth and certainly challenging, but not impossible. In the literature, few reports determine the polarity of the fabricated heterostructure: Hong *et al.* claim to achieve both ZnO polarities on Ga-polar GaN substrates by either Zn or O predeposition;[2] Liu *et al.* reported a nonpolar (m-plane) GaN/ZnO heterostructure[16] and Kobayashi *et al.* used O-polar ZnO substrates to grow both GaN polarities on top by changing the growth temperature.[29] However, for the latter situation, our simulations are not applicable as strain is obviously expected in the GaN region which would influence the piezoelectric charge distribution. In any case, the realization of p-GaN/n-ZnO heterojunctions with all polarity configurations seems to be possible; thus, a detailed understanding of the band alignments as presented above can be helpful to understand the experimental results.

Additionally, for a known polarity configuration, the strain sensitivity of these heterostructures can be exploited to intentionally manipulate the band structure by external strain. In this way, Yang *et al.* achieved an enhancement of the quantum efficiency,[7] whereas

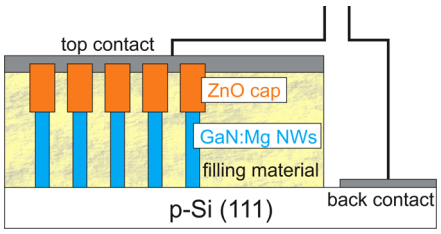

Figure 3. Schematic picture of the proposed p-GaN/n-ZnO heterostructure for the realization of an efficient LED emitting in the UV spectral range. Mg-doped GaN NWs are grown on silicon and subsequently overgrown with ZnO, which is intrinsically n-type. The NWs are spin-coated with a transparent and insulating material, subsequently etched down to reveal the ZnO tips and contacted by a semitransparent top contact.

Pan *et al.* used this effect on electroluminescence for sensing pressure distributions.[30]

RESULTS AND DISCUSSION

The second part of this article is dedicated to the characterization of a model interface, where a nanowire geometry is chosen to minimize the presence of defects in the interesting interface region. For this purpose, p-GaN nanowires were overgrown by intrinsically n-type ZnO to form a pn-heterojunction which might be used as LED emitting in the UV-spectral range according to Figure 3.

The heterojunction nanowires were fabricated in a two-step growth procedure using two different MBE systems. A detailed description can be found in the Experimental Section. Figure 4a,b shows scanning electron microscopy (SEM) images of GaN:Mg NWs which were deposited on p-type silicon (111) according to Furtmayr *et al.*[31] The dimensions of the p-type doped GaN NWs were determined to be 40 $\pm$ 8 nm in diameter and 360 $\pm$ 30 nm in length. After the second growth step, ZnO coverage can clearly be seen while maintaining the NW geometry by high axial and low radial growth rates (Figure 4b,d). In scanning transmission electron microscopy (STEM) studies, the formation of ZnO caps with a mean height of 200 nm is observed on almost all polar GaN NW top facets. However, only part of the nonpolar side facets are covered by a complete ZnO shell with thicknesses up to 20 nm, extending toward the bottom of the NW. The others show the formation of a homogeneous Ga_2O_3 layer of several nanometers which seems to prevent ZnO nucleation.

A detailed analysis of the GaN/ZnO heterointerface was performed by means of atomic resolution high-angle annular dark field (HAADF) STEM in combination with electron energy loss spectroscopy (EELS) which is presented in Figure 5 (top). Here, a sample with thinner ZnO coverage was used for a better access to the interface region. The polar top facet of an exemplary GaN NW is covered with a ZnO cap, which is slightly larger in diameter. Interestingly, the ZnO cap does not sit exclusively on the GaN top facet, but surrounds the

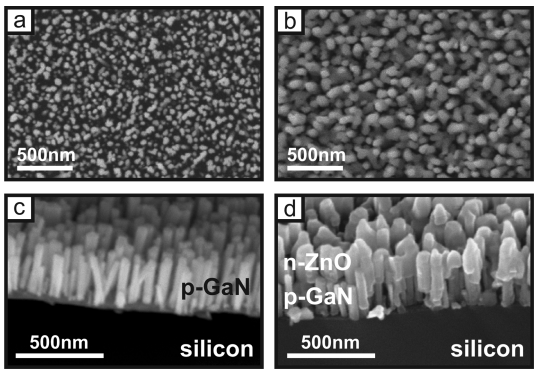

Figure 4. Top-view and tilted-view SEM images of p-GaN NWs grown on silicon substrate before (a and c) and after (b and d) ZnO overgrowth.

GaN NW for about 10 nm. As previously mentioned, the NW sidewalls are not covered with ZnO but with a 1−5 nm thick crystalline Ga_2O_3 layer with a nitrogen content of up to 20% (substitutional for O, Supporting Information). This indicates that the mobility of the impinging Zn atoms is high enough to reach the polar top facet of the GaN NWs, whereas the impinging oxygen radicals are incorporated also on the nonpolar sidewalls and form Ga_2O_3.

The heterointerface in the HAADF STEM image is smooth and abrupt with no defects to be seen in the vicinity, what is clearly a result of the low lattice mismatch of the two materials. A separation of GaN and ZnO by an intermediate Ga_2O_3 layer is not observed. As discussed previously, it is crucial to know the polarity configuration to model the electronic band structure across the heterostructure. Therefore, the polarities of GaN and ZnO were determined in a direct way by aberration-corrected annular bright field (ABF) STEM.[32−34] The results (Figure 5, bottom) reveal the characteristic double layers in polar direction where the single dumbbells are clearly resolved. From this, the polarity can be determined to be N-polar for GaN and Zn-polar for ZnO. This polarity inversion from anion to cation was found to occur for all investigated heterojunction nanowires. The attempt to influence the ZnO polarity by the growth procedure, *i.e.*, starting the growth with Zn or O preexposure, was investigated in two additional samples but showed no effect on the polarity configuration. This can be assigned to the high binding energy of the N−O bonds which seem to be responsible for the observed polarity inversion. According to the corresponding simulation of the band structure, a confinement of electrons in a 2DEG on the ZnO-side of the interface is expected (Figure 2d).

The optical properties of the heterojunction NWs were investigated by ensemble photoluminescence (PL) in backscattering geometry with an excitation wavelength of 244 nm. The PL spectrum at liquid-helium temperature is presented in Figure 6a over a wide energy range, where only ZnO-related luminescence is

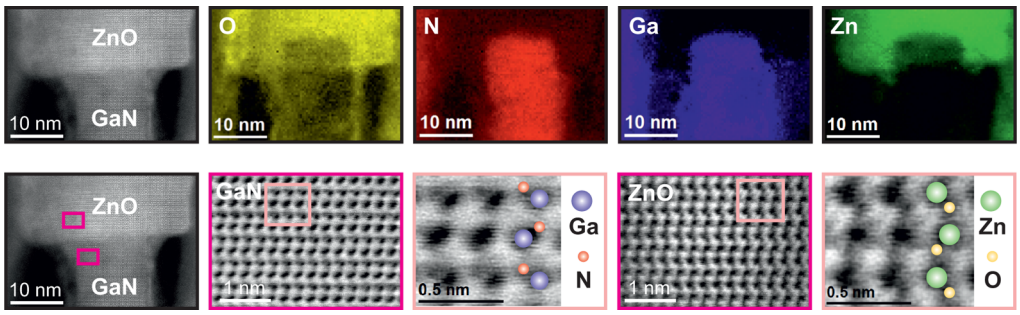

Figure 5. The HAADF STEM image (left) of an exemplary p-GaN/n-ZnO heterojunction nanowire reveals a high-quality interface region. EELS maps identify the different atomic species O, N, Ga, and Zn (top row, 2−5). In aberration-corrected ABF STEM, a polarity inversion is observed from N-polar GaN to Zn-polar ZnO (bottom row, 2−5).

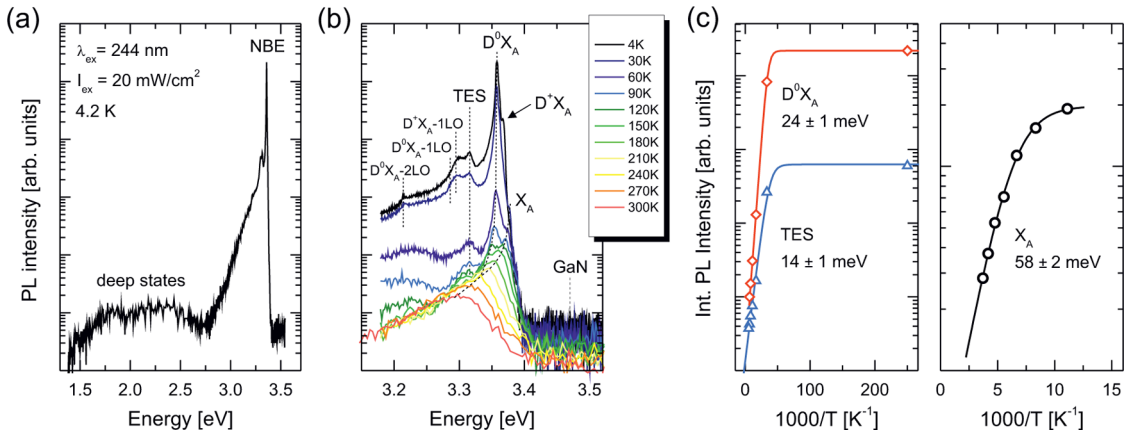

Figure 6. (a) Ensemble PL spectrum at 4.2 K of p-GaN/n-ZnO heterojunction NWs over a wide energy range showing an intense excitonic emission (NBE) at 3.358 eV. (b) Temperature dependence of the PL emission in the NBE region from 4.2 K to room temperature. (c) The intensity quenching for D^0X_A, TES and X_A is displayed in an Arrhenius plot with the calculated activation energies according to eq 1.

observed due to a complete absorption of the excitation laser in the ZnO caps. The spectrum can be divided in two relevant regions: (i) an intense excitonic near-band-gap emission (NBE, 3.2−3.4 eV) and (ii) defect-related luminescence bands in the energy range of 1.7−2.5 eV, often referred to as red, yellow and green luminescence bands.[23] As the latter show an intensity over 4 orders of magnitude lower, a high crystalline quality of the p-GaN/n-ZnO NWs can be confirmed, in accordance with the HAADF and ABF STEM results presented above (Figure 5).

To identify the origin of the single emission lines in the NBE region, a temperature-dependent measurement was performed from 4.2 to 300 K (Figure 6b). Besides the energy position, the intensity quenching of a PL emission line is characteristic for the responsible recombination process. This temperature-induced drop in PL intensity can be modeled according to Bimberg *et al.*[35] by the onset of a nonradiative process with an activation energy E_a:

$$I(T) = \frac{I_0}{1 + C \cdot \exp\left(-\frac{E_a}{kT}\right)} \quad (1)$$

The integrated PL peak intensities of the emission lines denoted with D^0X_A, TES, and X_A are fitted in Figure 6c according to this model and the deduced activation energies are given in Table 2.

TABLE 2. Summary of Observed PL Emission Lines with Deduced Activation Energies According to eq 1

	energy [eV]	act. energy [meV]
X_A	3.377	58 ± 2
D^+X_A	3.367	n/a
D^0X_A	3.358	24 ± 1
TES	3.316	14 ± 1
D^+X_A − 1LO	3.295	n/a
D^0X_A − 1LO	3.286	n/a
D^0X_A − 2LO	3.214	n/a

In the following, energy positions and activation energies are used to identify the origin of the observed PL emissions. At low temperatures, the most intense emission is located at 3.358 eV, accompanied by LO phonon replicas at 3.286 and 3.214 eV, and can be assigned to neutral donor-bound exciton recombination (D^0X_A). In this context, the nonradiative process with an activation energy of 24 ± 1 meV can be understood as the dissociation of bound excitons from the donors. In fact, there are two reasonable candidates for the origin of the donors: indium contamination from the

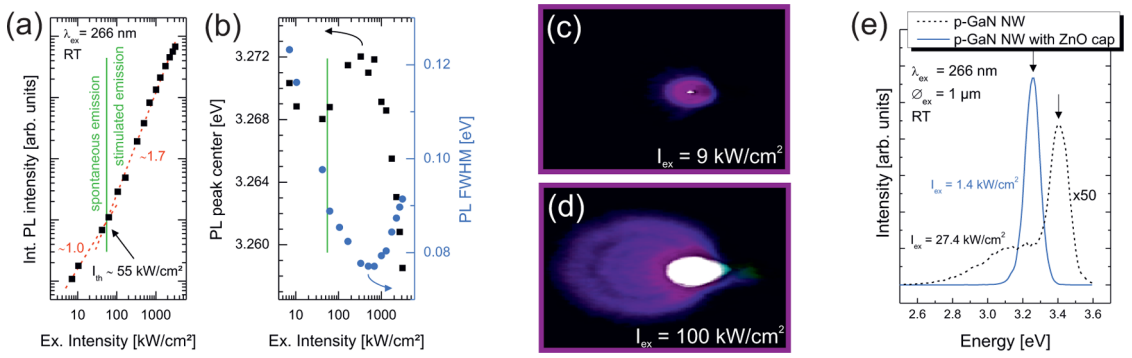

Figure 7. (a) μPL excitation of an ensemble of approximately 200 p-GaN/n-ZnO heterojunction NWs at room temperature. The double-logarithmic slope of the integrated PL peak intensity indicates a transition from spontaneous to stimulated emission at a certain threshold value. (b) Corresponding PL peak center and fwhm. (c and d) The excitation of a single heterojunction NW dispersed on glass can be observed in a webcam and shows strong UV emission (c) below and (d) above threshold. (e) The spectra of a single p-GaN NW before and after ZnO overgrowth are presented, where the emission in the heterojunction NW can clearly be assigned to the ZnO region.

gluing of the sample onto the sample holder or the presence of gallium from the p-GaN NWs in the vicinity of the interface. The responsible donor can be identified by the observation of the associated two-electron-satellite (TES), which exhibits a characteristic separation energy with respect to the D^0X_A. Here, the TES is observed at 3.316 eV with an activation energy of 14 ± 1 meV. The resulting energy separation of 42 meV has been reported by Meyer *et al.* for gallium donors in ZnO.[36] Consistently, the emission line at 3.367 eV and its first order phonon replica, which are visible only at low temperatures, can be identified as ionized donor-bound exciton recombination involving the same gallium donors (D^+X_A).[36]

At a slightly higher energy of 3.377 eV, the free A-exciton recombination (X_A) is observed, which is weak in intensity compared to D^0X_A because of a fast capture at gallium impurities and reabsorption effects. For increasing temperature, however, the free exciton recombination starts to dominate the spectrum as donor-bound excitons can overcome the localization energy. The deduced X_A activation energy of 58 ± 2 meV can be identified as exciton binding energy in ZnO which is in accordance with literature values.[37]

As presented previously, an electron accumulation at the ZnO-side of the interface is predicted by the performed band structure simulations in p-GaN/n-ZnO heterojunction NWs with the deduced N-polar/Zn-polar configuration (Figure 2d). The PL results above show three remarkable features supporting these band structure simulations: (i) the identification of luminescence related to gallium donors which are present only in the vicinity of the interface, (ii) the observation of the corresponding TES up to comparatively high temperatures, and (iii) the presence of the first order phonon replica for ionized donor-bound excitons ($D^+X_A - 1LO$). These are indications for a high electron concentration in the investigated structure with the interface being the only reasonable location.

The high exciton binding energy of 59 meV in ZnO could prove advantageous with respect to GaN homodiodes in the field of high-power optoelectronic devices operating at elevated temperatures. Thus, the performance of the NWs under strong optical excitation at room temperature was investigated by μPL, optically pumped by a 266 nm continuous-wave laser system. To achieve high power densities, the excitation laser was focused on the sample through a UV objective to reduce the spot size to a diameter of about 1 μm.

The integrated μPL peak intensity for increasing excitation densities is presented in Figure 7a for simultaneous excitation of an ensemble of about 200 NWs. In the low-excitation regime, a linear increase with a double-logarithmic slope of 1.0 is observed which is characteristic for spontaneous emission with negligible nonradiative losses. When exceeding the graphically determined threshold value of 55 kW/cm^2, the μPL intensity is found to increase superlinearly with a slope of 1.7, revealing the onset of stimulated emission. Remarkably, no drop in stimulated emission is observed up to an extremely high excitation density of 3 MW/cm^2, which is the maximum of the laser system used. In other words, the temperature of thermal dissociation of excitons in ZnO could not be reached within the heterojunction NWs. The corresponding PL peak center shows an S-shape behavior (Figure 7b) which can be interpreted in the following way: (i) a red-shift in the low-excitation regime due to a temperature-induced shrinkage of the bandgap; (ii) a blue-shift in the moderate-excitation regime starting at the threshold value, indicating the onset of stimulated emission; (iii) a red-shift in the high-excitation regime where strong heating takes place. The PL fwhm supports this interpretation, as it decreases continuously with upcoming stimulated emission, until the effect of thermal broadening of the PL emission dominates.

To investigate the performance of single NWs, they were released from the silicon substrate and dispersed

in a low density on a nonfluorescent glass plate. In a webcam, intense UV emission of a single NW can be observed for a low excitation density with the radial symmetry indicating spontaneous emission (Figure 7c). For an excitation density above threshold the UV emission drastically increases due to stimulated emission (Figure 7d). This affects also the emission symmetry, as the NWs represent intrinsic waveguides due to a high refractive index. A preferred emission along the axial direction of the NW is clearly observed, where interference fringes prove the presence of stimulated emission. The side where the emission leaves the NW is presumably the top where the ZnO cap is located.

In Figure 7e, the μPL spectra of a single p-GaN NW is compared to a single heterojunction NW. The p-GaN NW shows a GaN bandgap emission at 3.40 eV and a broad luminescence at 2.7−3.3 eV which can be assigned to the high density of Mg acceptors (Figure 7e). After ZnO overgrowth, much lower excitation densities are needed to get high emission rates. The corresponding spectrum reveals an intense emission at 3.26 eV originating from the ZnO cap. Even though the p-GaN part was simultaneously excited in the lying NW, no emission from this region could be detected anymore.

The optical investigations clearly demonstrate the advantage of p-GaN/n-ZnO heterojunction NWs, in particular a low threshold for stimulated emission. A variation of the threshold values for different NWs was found to be in a wide range of 1−100 kW/cm^2, probably influenced by the actual NW geometry. With respect to device fabrication, an optimization of the geometry, *e.g.*, the NW length and the ZnO cap thickness, seems promising to further decrease the threshold and increase the emission efficiency. A specific design of the NWs to form intrinsic cavities can be an easy route for high efficiency heterojunction nanowire laser diodes. Thus, the challenge of further work will be the fabrication of the proposed model device according to Figure 3 in order to achieve electrically injected emission.

CONCLUSION

In this article, a systematic analysis of the p-GaN/n-ZnO heterojunction has been presented. Simulations showed the electronic band structure to be strongly dependent on the polarity of the two wurtzite materials. As a model structure, p-GaN nanowires were capped by ZnO to form an ideal heterostructure where the polarity was found to be inverted from N-polar GaN to Zn-polar ZnO. These heterojunction NWs showed outstanding optical properties, *e.g.*, strong stimulated emission with a low threshold, which make them a promising approach for high efficiency LEDs and laser diodes emitting in the UV spectral range.

EXPERIMENTAL SECTION

Self-assembled p-GaN NWs were grown on silicon substrates by plasma-assisted molecular beam epitaxy (PAMBE). In advance, the native oxide layer of low-resistive p-type Si(111) substrates was removed by a HF etching step (5%, 30 s). Subsequently, the nanowire growth was performed in an UHV environment, where Ga and Mg were provided by standard effusion cells and nitrogen radicals were supplied by an Oxford Applied Research RF plasma source operated at 425 W. According to Furtmayr *et al.*,[31] the Ga and N fluxes were fixed to 2.5×10^{-7} mbar beam equivalent pressure (BEP) and 0.9 sccm, respectively. Additionally, a Mg dopant flux of 3.0×10^{-10} mbar BEP was applied to ensure a sufficiently high acceptor concentration in the GaN NWs, which is estimated to be in the range of 10^{19} cm^{-3}. The substrate temperature was adjusted to 775 °C according to pyrometer measurement. The growth process was started by a nitridation of the silicon substrates for 10 min.

In a second step, the p-GaN NWs were transferred to another PAMBE system for ZnO overgrowth, where UHV conditions had to be left for several minutes. A double-zone effusion cell was used for evaporating Zn while oxygen radicals were provided by an Oxford Applied Research RF plasma source operated at 400 W. The Zn and O fluxes were fixed at 1.0×10^{-7} mbar BEP and 0.6 sccm, respectively. An elevated substrate temperature of 540 °C was applied to ensure a high quality of the ZnO.

The morphology of the samples was investigated by scanning electron microscopy (SEM, Zeiss NVision40). Direct polarity measurements[32] were performed by atomic resolution aberration-corrected annular bright field scanning transmission electron microscopy imaging (ABF STEM) in a probe corrected FEI Titan 60−300 keV microscope operated at 300 keV. This latter technique was found to be useful in order to directly determine polarity in NWs even when one of the elements composing the structure is light,[32] as in the case of ZnO[33] and GaN,[34] respectively. HAADF-STEM imaging and STEM-EELS chemical mapping were also carried out in a probe corrected FEI Titan 60−300 at 300 keV.

Photoluminescence was measured in backscattering geometry with a continuous-wave frequency-doubled argon ion laser operating at 244 nm excitation wavelength. The focal diameter was about 1 mm which means that a large ensemble of NWs was simultaneously excited. For temperature-dependent measurements, the sample was mounted in a contact gas cryostat and cooled with liquid helium. The signal was collected in a DILOR double spectrometer (focal length 800 mm, resolution 0.05 nm) and detected by a photomultiplier tube. For μPL at room temperature, the 266 nm Nd:YAG laser line (cw) was focused through a 40× UV-objective (NA = 0.5) on the sample, resulting in a spot diameter of approximately 1 μm. To measure single NWs, they were released from the substrate in acetone and dispersed on a nonluminescent quarz glass plate.

Conflict of Interest: The authors declare no competing financial interest.

Acknowledgment. Financial support from the Deutsche Forschungsgemeinschaft (DFG) *via* the Forschergruppe 1493, TUM.solar in the frame of the Bavarian Collaborative Research Project "Solar Technologies go Hybrid" (SolTec) and the Excellence Cluster Nanosystems Initiative Munich is gratefully acknowledged. J.A. and R.R.Z. acknowledge the funding from the Spanish MICINN project MAT2010-15138 (COPEON) and MAT2010-21510, Generalitat de Catalunya 2009 SGR 770 and the TEM facilities at INA-LMA (Univ. Zaragoza). Authors acknowledge F.J. Belarre for STEM X-section sample preparation.

Supporting Information Available: Details of the Ga_2O_3 shell are presented. This material is available free of charge *via* the Internet at http://pubs.acs.org.

REFERENCES AND NOTES

1. Vispute, R. D.; Talyansky, V.; Choopun, S.; Sharma, R. P.; Venkatesan, T.; He, M.; Tang, X.; Halpern, J. B.; Spencer, M. G.; Li, Y. X.; *et al.* Heteroepitaxy of ZnO on GaN and its Implications for Fabrication of Hybrid Optoelectronic Devices. *Appl. Phys. Lett.* **1998**, *73*, 348–350.
2. Hong, S.-K.; Hanada, T.; Ko, H.-J.; Chen, Y.; Yao, T.; Imai, D.; Araki, K.; Shinohara, M. Control of Polarity of ZnO Films Grown by Plasma-Assisted Molecular Beam Epitaxy: Zn- and O-Polar ZnO Films on Ga-Polar GaN Templates. *Appl. Phys. Lett.* **2000**, *77*, 3571–3573.
3. Hamdani, F.; Yeadon, M.; Smith, D. J.; Tang, H.; Kim, W.; Salvador, A.; Botchkarev, A. E.; Gibson, J. M.; Polyakov, A. Y.; Skowronski, M.; *et al.* Microstructure and Optical Properties of Epitaxial GaN on ZnO (0001) Grown by Reactive Molecular Beam Epitaxy. *J. Appl. Phys.* **1998**, *83*, 983–990.
4. Alivov, Y. I.; Van Nostrand, J. E.; Look, D. C.; Chukichev, M. V.; Ataev, B. M. Observation of 430 nm Electroluminescence from ZnO/GaN Heterojunction Light-Emitting Diodes. *Appl. Phys. Lett.* **2003**, *83*, 2943–2945.
5. Park, W.; Yi, G.-C. Electroluminescence in n-ZnO Nanorod Arrays Vertically Grown on p-GaN. *Adv. Mater.* **2004**, *16*, 87–90.
6. Rogers, D. J.; Hosseini Teherani, F.; Yasan, A.; Minder, K.; Kung, P.; Razeghi, M. Electroluminescence at 375nm from a ZnO/GaN:Mg/c-Al_2O_3 Heterojunction Light-Emitting Diode. *Appl. Phys. Lett.* **2006**, *88*, 141918.
7. Yang, Q.; Wang, W.; Xu, S.; Wang, Z. L. Enhancing Light Emission of ZnO Microwire-Based Diodes by Piezo-Phototronic Effect. *Nano Lett.* **2011**, *11*, 4012–4017.
8. Jeong, M.-C.; Oh, B.-Y.; Ham, M.-H.; Lee, S.-W.; Myoung, J.-M. ZnO-Nanowire-Inserted GaN/ZnO Heterojunction Light-Emitting Diodes. *Small* **2007**, *3*, 568–572.
9. Zhang, X.-M.; Lu, M.-Y.; Zhang, Y.; Chen, L.-J.; Wang, Z. L. Fabrication of a High-Brightness Blue-Light-Emitting Diode Using a ZnO-Nanowire Array Grown on p-GaN Thin Film. *Adv. Mater.* **2009**, *21*, 2767–2770.
10. Myoung, J. M.; Shim, K. H.; Kim, C.; Gluschenkov, O.; Kim, K.; Kim, S.; Turnbull, D. A.; Bishop, S. G. Optical Characteristics of p-Type GaN Films Grown by Plasma-Assisted Molecular Beam Epitaxy. *Appl. Phys. Lett.* **1996**, *69*, 2722–2724.
11. Xu, H. Y.; Liu, Y. C.; Liu, Y. X.; Xu, C. S.; Shao, C. L.; Mu, R. Ultraviolet Electroluminescence from p-GaN/i-ZnO/n-ZnO Heterojunction Light-Emitting Diodes. *Appl. Phys. B: Lasers Opt.* **2005**, *80*, 871–874.
12. Guo, R.; Nishimura, J.; Matsumoto, M.; Higashihata, M.; Nakamura, D.; Okada, T. Electroluminescence from ZnO Nanowire-Based p-GaN/n-ZnO Heterojunction Light-Emitting Diodes. *Appl. Phys. B: Lasers Opt.* **2009**, *94*, 33–38.
13. Birner, S.; Zibold, T.; Andlauer, T.; Kubis, T.; Sabathil, M.; Trellakis, A.; Vogl, P. Nextnano: General Purpose 3-D Simulations. *IEEE Trans. Electron Devices* **2007**, *54*, 2137–2142.
14. Van de Walle, C. G.; Neugebauer, J. Universal Alignment of Hydrogen Levels in Semiconductors, Insulators and Solutions. *Nature* **2003**, *423*, 626–628.
15. Hong, S.-K.; Hanada, T.; Makino, H.; Chen, Y.; Ko, H.-J.; Yao, T.; Tanaka, A.; Sasaki, H.; Sato, S. Band Alignment at a ZnO/GaN (0001) Heterointerface. *Appl. Phys. Lett.* **2001**, *78*, 3349–3351.
16. Liu, J. W.; Kobayashi, A.; Toyoda, S.; Kamada, H.; Kikuchi, A.; Ohta, J.; Fujioka, H.; Kumigashira, H.; Oshima, M. Band Offsets of Polar and Nonpolar GaN/ZnO Heterostructures Determined by Synchrotron Radiation Photoemission Spectroscopy. *Phys. Status Solidi B* **2011**, *248*, 956–959.
17. Li, J.; Oder, T. N.; Nakarmi, M. L.; Lin, J. Y.; Jiang, H. X. Optical and Electrical Properties of Mg-Doped p-Type $Al_xGa_{1-x}N$. *Appl. Phys. Lett.* **2002**, *80*, 1210–1212.
18. Hofmann, D. M.; Hofstaetter, A.; Leiter, F.; Zhou, H.; Henecker, F.; Meyer, B. K.; Orlinskii, S. B.; Schmidt, J.; Baranov, P. G. Hydrogen: A Relevant Shallow Donor in Zinc Oxide. *Phys. Rev. Lett.* **2002**, *88*, 045504.
19. Polian, A.; Grimsditch, M.; Grzegory, I. Elastic Constants of Gallium Nitride. *J. Appl. Phys.* **1996**, *79*, 3343–3344.
20. Vurgaftman, I.; Meyer, J. R. Band Parameters for Nitrogen-Containing Semiconductors. *J. Appl. Phys.* **2003**, *94*, 3675–3696.
21. Laumer, B.; Schuster, F.; Stutzmann, M.; Bergmaier, A.; Dollinger, G.; Eickhoff, M. Accurate Determination of Optical Bandgap and Lattice Parameters of $Zn_{1-x}Mg_xO$ Epitaxial Films ($0 < x < 0.3$) Grown by Plasma-assisted Molecular Beam Epitaxy on a-Plane Sapphire. *J. Appl. Phys.* **2013**, *113*, 233512.
22. Ambacher, O. Growth and Applications of Group III-Nitrides. *J. Phys. D: Appl. Phys.* **1998**, *31*, 2653.
23. Özgür, U.; Alivov, Y. I.; Liu, C.; Teke, A.; Reshchikov, M. A.; Doğan, S.; Avrutin, V.; Cho, S.-J.; Morkoç, H. A Comprehensive Review of ZnO Materials and Devices. *J. Appl. Phys.* **2005**, *98*, 041301.
24. Lambrecht, W. R. L.; Rodina, A. V.; Limpijumnong, S.; Segall, B.; Meyer, B. K. Valence Band Ordering and Magneto-Optic Exciton Fine Structure in ZnO. *Phys. Rev. B* **2002**, *65*, 075207.
25. Ioffe Physical Technical Institute. 2013; http://www.ioffe.rssi.ru/SVA/NSM/Semicond/GaN/bandstr.html.
26. Ashkenov, N.; Mbenkum, B. N.; Bundesmann, C.; Riede, V.; Lorenz, M.; Spemann, D.; Kaidashev, E. M.; Kasic, A.; Schubert, M.; Grundmann, M.; *et al.* Infrared Dielectric Functions and Phonon Modes of High-Quality ZnO Films. *J. Appl. Phys.* **2003**, *93*, 126–133.
27. Noel, Y.; Zicovich-Wilson, C. M.; Civalleri, B.; D'Arco, P.; Dovesi, R. Polarization Properties of ZnO and BeO: An *ab Initio* Study Through the Berry Phase and Wannier Functions Approaches. *Phys. Rev. B* **2001**, *65*, 014111.
28. Gopal, P.; Spaldin, N. Polarization, Piezoelectric Constants, and Elastic Constants of ZnO, MgO, and CdO. *J. Electr. Mater.* **2006**, *35*, 538–542.
29. Kobayashi, A.; Kawaguchi, Y.; Ohta, J.; Fujioka, H.; Fujiwara, K.; Ishii, A. Polarity Control of GaN Grown on ZnO (000−1) Surfaces. *Appl. Phys. Lett.* **2006**, *88*, 181907.
30. Pan, C.; Dong, L.; Zhu, G.; Niu, S.; Yu, R.; Yang, Q.; Liu, Y.; Wang, Z. L. High-Resolution Electroluminescent Imaging of Pressure Distribution Using a Piezoelectric Nanowire LED Array. *Nat. Photonics* **2013**, *7*, 752–758.
31. Furtmayr, F.; Vielemeyer, M.; Stutzmann, M.; Arbiol, J.; Estradé, S.; Peirò, F.; Morante, J. R.; Eickhoff, M. Nucleation and Growth of GaN Nanorods on Si (111) Surfaces by Plasma-Assisted Molecular Beam Epitaxy—The Influence of Si- and Mg-Doping. *J. Appl. Phys.* **2008**, *104*, 034309.
32. de la Mata, M.; Magen, C.; Gazquez, J.; Utama, M. I. B.; Heiss, M.; Lopatin, S.; Furtmayr, F.; Fernández-Rojas, C. J.; Peng, B.; Morante, J. R.; *et al.* Polarity Assignment in ZnTe, GaAs, ZnO, and GaN-AlN Nanowires from Direct Dumbbell Analysis. *Nano Lett.* **2012**, *12*, 2579–2586.
33. Utama, M. I. B.; Belarre, F. J.; Magen, C.; Peng, B.; Arbiol, J.; Xiong, Q. Incommensurate van der Waals Epitaxy of Nanowire Arrays: A Case Study with ZnO on Muscovite Mica Substrates. *Nano Lett.* **2012**, *12*, 2146–2152.
34. Schuster, F.; Furtmayr, F.; Zamani, R.; Magen, C.; Morante, J. R.; Arbiol, J.; Garrido, J. A.; Stutzmann, M. Self-Assembled GaN Nanowires on Diamond. *Nano Lett.* **2012**, *12*, 2199–2204.
35. Bimberg, D.; Sondergeld, M.; Grobe, E. Thermal Dissociation of Excitons Bounds to Neutral Acceptors in High-Purity GaAs. *Phys. Rev. B* **1971**, *4*, 3451–3455.
36. Meyer, B. K.; Alves, H.; Hofmann, D. M.; Kriegseis, W.; Forster, D.; Bertram, F.; Christen, J.; Hoffmann, A.; Strassburg, M.; Dworzak, M.; *et al.* Bound Exciton and Donor-Acceptor Pair Recombinations in ZnO. *Phys. Status Solidi B* **2004**, *241*, 231–260.
37. Thomas, D. G. The Exciton Spectrum of Zinc Oxide. *J. Phys. Chem. Solids* **1960**, *15*, 86–96.